Lattice Boltzmann simulations of segregating binary fluid mixtures in shear flow

A. Lamura[a,b,*], G. Gonnella[a]

[a]*Istituto Nazionale per la Fisica della Materia, Unità di Bari, Dipartimento di Fisica dell'Università di Bari, Istituto Nazionale di Fisica Nucleare, Sezione di Bari via Amendola 173, 70126 Bari, Italy*
[b]*Institut für Festkörperforschung, Forschungszentrum Jülich, 52425 Jülich, Germany*

Abstract

We apply lattice Boltzmann method to study the phase separation of a two-dimensional binary fluid mixture in shear flow. The algorithm can simulate systems described by the Navier–Stokes and convection–diffusion equations. We propose a new scheme for imposing the shear flow which has the advantage of preserving mass and momentum conservation on the boundary walls without introducing slip velocities. We study how the steady velocity profile is reached. Our main results show the presence of two typical length scales in the phase separation process, corresponding to domains with two different thicknesses. © 2001 Elsevier Science B.V. All rights reserved.

PACS: 64.75.+g; 47.11.+j; 83.10.Lk

Keywords: Lattice Boltzmann equations; Nonslip boundary conditions; Computer simulations; Binary fluid mixtures; Phase separation

1. Introduction

When a fluid mixture is suddenly quenched from a disordered initial condition to a coexistence state below the critical temperature, the two fluids segregate with domains growing with time (see, e.g., Ref. [1]). The morphology of these domains is strongly influenced by an applied flow. In the case of a shear flow (for a review see Ref. [2]), the domains are observed to grow greatly elongated in the flow direction (see, e.g.,

---
* Correspondence address. Institut für Festkörperforschung, Forschungszentrum Jülich, 52425 Jülich, Germany. Tel.: ++49-2461-616290; fax: ++49-2461-612850.
E-mail address: a.lamura@fz-juelich.de (A. Lamura).

Ref. [3]). The effects of the shear have been considerably investigated in the last years. Several numerical simulations confirm the anisotropic growth of the domains [4–10]. New recent theoretical results by Corberi et al. [11,12] show that, as an effect of the shear, the mixture contains domains of two different thicknesses and that the relative abundance of these domains changes periodically with the logarithm of time. However, in the papers of Corberi et al. [11,12] phase separation occurred only for the effects of simple diffusion. The main purpose of this paper is to see how the hydrodynamics affects this picture.

The presence of domains with different scales is a very peculiar result for phase separating mixtures. Indeed, in the general picture for the unsheared case, a single time-dependent length scale $R(t)$, which measures the typical size of domains, characterizes the behaviour of the mixture (see [13]). This length grows with the power-law $R(t) \sim t^\alpha$, where the value of the growth exponent α is strictly related to the physical mechanism operating in the segregation process. For example, $\alpha = \frac{1}{3}$ in a pure diffusive regime. Therefore, the existence of two characteristic scales makes the phase separation process very interesting from a theoretical point of view and also with relevant practical implications.

Looking at the effects of hydrodynamics on this problem is not a simple computational task. Domains grow fast in the direction of the flow making finite-size effects quite soon relevant in simulations (for a recent review, see Refs. [14,15]). In this paper, we use a lattice Boltzmann scheme [16,17] to simulate the convection–diffusion and Navier–Stokes equations for a binary mixture. This method has been found very convenient with respect to other numerical algorithms for fluid mixtures [18] since it allows to reach very large time scales. In particular, an advantage of the lattice Boltzmann scheme of Orlandini et al. [16] and Swift et al. [17], is that the correct fluid equilibrium can be imposed by choosing an appropriate free energy. Moreover, differently from other lattice gas methods, it allows to control in a separate way the different mechanisms of transport tuning independently the fluid viscosity and the diffusivity. The mentioned lattice Boltzmann scheme has been used with success in several problems of phase separation of binary fluid mixtures without shear in two [19] and three dimensions [20], and also in the case of complex fluids [21].

A preliminary important part of our work has been to include proper boundary conditions for a shear flow in lattice Boltzmann schemes. This problem has been studied in many papers on lattice Boltzmann schemes for a single fluid (for a review, see, e.g., Ref. [18]) and for binary mixtures by Wagner and Yeomans [22] and Cates et al. [23]. We discuss previous procedures and propose an improved algorithm which allows to strictly conserve mass and momentum on the boundary walls without introducing slip velocities.

The outline of the paper is as follows. In the next section, we describe the fluid model and the lattice Boltzmann scheme. In Section 3, we describe and compare different approaches for implementing shear boundary conditions in the numerical scheme. In Section 4, we give our results for the phase separation and finally we draw our conclusions.

2. The lattice Boltzmann method

Our simulations are based on a lattice Boltzmann scheme developed by Orlandini et al. [16] and Swift et al. [17]. In this scheme, the choice of a free energy determines all the thermodynamic properties of the fluid. We start from the description of the free energy of the fluid mixture; then we show how the lattice Boltzmann equations have been implemented.

2.1. Equilibrium description of the mixture

The free-energy functional generally used in phase separation studies of binary mixtures [13] is

$$\mathscr{F} = \int d\mathbf{r} \left[\frac{a}{2}\varphi^2 + \frac{b}{4}\varphi^4 + \frac{\kappa}{2}(\nabla\varphi)^2 \right] , \tag{1}$$

where φ is the order parameter which describes the normalized difference in the densities of the two fluids. The polynomial terms are related to the bulk properties of the fluid. While the parameter b is always positive, the sign of a distinguishes between a disordered and a segregated mixture. The case with $a > 0$ gives a polynomial with one minimum in the origin corresponding to the a state with $\varphi = 0$ everywhere while two minima are present when $a < 0$ corresponding to the two pure phases with $\varphi = \pm\sqrt{-a/b}$. In the following, we will consider a deep quench (well below the critical value $a = 0$) into the coexistence region with $a = -1$ and $b = 1$. The gradient term is related to the interfacial properties. The equilibrium profile between the two coexisting bulk phases is $\varphi(x) = \tanh\sqrt{(1/2\kappa)}x$ giving a surface tension equal to $\frac{2}{3}\sqrt{2\kappa}$ and an interfacial width proportional to $\sqrt{2\kappa}$ [24]. The total fluid density n is not explicitly included in Eq. (1) because we are dealing with an incompressible mixture with n constant throughout the volume of the fluid and throughout its motion.

The thermodynamic properties of the fluid follow from the free energy (1). The chemical potential difference between the two fluids is given by

$$\Delta\mu = \frac{\delta\mathscr{F}}{\delta\varphi} = a\varphi + b\varphi^3 - \kappa\nabla^2\varphi . \tag{2}$$

The pressure is not a scalar but a tensor $P_{\alpha\beta}$ since interfaces in the fluid can exert non-isotropic forces [25]. The scalar part p_0 follows directly from Eq. (1):

$$p_0 = \varphi\frac{\delta\mathscr{F}}{\delta\varphi} - f(\varphi)$$

$$= \frac{a}{2}\varphi^2 + \frac{3b}{4}\varphi^4 - \kappa\varphi(\nabla^2\varphi) - \frac{\kappa}{2}(\nabla\varphi)^2 , \tag{3}$$

where $f(\varphi)$ is the free-energy density. In order to calculate the pressure tensor $P_{\alpha\beta}$, one has to ensure that $P_{\alpha\beta}$ obeys the condition of mechanical equilibrium $\partial_\alpha P_{\alpha\beta} = 0$ [26]. A suitable choice is

$$P_{\alpha\beta} = p_0\delta_{\alpha\beta} + \kappa\partial_\alpha\varphi\partial_\beta\varphi . \tag{4}$$
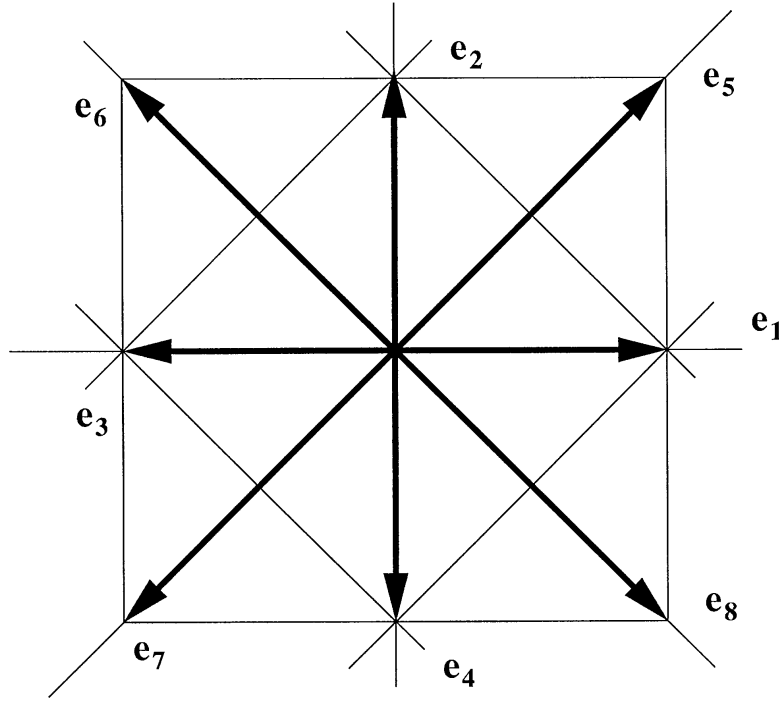
Fig. 1. One plaquette of the lattice used in our model with the velocity vectors $\mathbf{e}_i$ ($\Delta t = 1$).

2.2. Lattice Boltzmann scheme

We use a square lattice in which each site has eight nearest neighbours. The lattice has horizontal and vertical links of unit length and diagonal links of length $\sqrt{2}$. We denote by L the number of lattice sites in each direction. The variables of the lattice Boltzmann algorithm are two sets of distribution functions $f_i(\mathbf{r}, t)$ and $g_i(\mathbf{r}, t)$, defined on each lattice site $\mathbf{r}$ at time t. Each of them is associated with a velocity vector $\mathbf{e}_i$. Defined Δt as the simulation time step, the quantities $\mathbf{e}_i \Delta t$ are constrained to be lattice vectors $|\mathbf{e}_i|\Delta t = 1$ for the horizontal and vertical directions ($i = 1, 2, 3, 4$) and $|\mathbf{e}_i|\Delta t = \sqrt{2}$ for the diagonal directions ($i = 5, 6, 7, 8$). In Fig. 1, we show a plaquette of the lattice with the velocity vectors. Two functions $f_0(\mathbf{r}, t)$ and $g_0(\mathbf{r}, t)$, corresponding to the distribution components that do not propagate ($\mathbf{e}_0 = \mathbf{0}$), are also taken into account.

The distribution functions are related to the total density n, to the fluid velocity $\mathbf{u}$ and to the density difference φ through

$$n = \sum_i f_i, \quad n\mathbf{u} = \sum_i f_i \mathbf{e}_i, \quad \varphi = \sum_i g_i . \tag{5}$$

They evolve during the time step Δt according to a single relaxation-time Boltzmann equation [27,28]:

$$f_i(\mathbf{r} + \mathbf{e}_i\Delta t, t + \Delta t) - f_i(\mathbf{r}, t) = -\frac{1}{\tau}[f_i(\mathbf{r}, t) - f_i^{eq}(\mathbf{r}, t)] , \tag{6}$$

$$g_i(\mathbf{r} + \mathbf{e}_i\Delta t, t + \Delta t) - g_i(\mathbf{r}, t) = -\frac{1}{\tau_\varphi}[g_i(\mathbf{r}, t) - g_i^{eq}(\mathbf{r}, t)] , \tag{7}$$

where τ and τ_φ are independent relaxation parameters, $f_i^{eq}(\mathbf{r},t)$ and $g_i^{eq}(\mathbf{r},t)$ are local equilibrium distribution functions.

The time evolution occurs in two steps: a collision and a propagation step. Firstly, the distribution functions arriving at the same time on the same site change according to the equation (we will write it only for one of the two distributions)

$$f_i^c(\mathbf{r},t) = f_i(\mathbf{r},t) - \frac{1}{\tau}[f_i(\mathbf{r},t) - f_i^{eq}(\mathbf{r},t)] . \tag{8}$$

Then the distribution functions are moved along the lattice directions according to the rule

$$f_i(\mathbf{r} + \mathbf{e}_i\Delta t, t + \Delta t) = f_i^c(\mathbf{r},t) . \tag{9}$$

Eq. (6) comes by combining Eqs. (8) and (9).

The system is initialized with $n = 1$, $\varphi = 0$ and $\mathbf{u} = \mathbf{0}$ everywhere. The choice of a constant value of n is justified by the incompressibility of the mixture. Our simulations confirm that n stays constant throughout the system during all the time evolutions. The initial value of φ corresponds to a symmetric $50:50$ mixture with the two fluids completely mixed. These quantities are locally conserved in any collision process and, therefore, we require that the local equilibrium distribution functions fulfil the following equations:

$$\sum_i (f_i^{eq} - f_i) = 0 \Rightarrow \sum_i f_i^{eq} = n ,$$

$$\sum_i (g_i^{eq} - g_i) = 0 \Rightarrow \sum_i g_i^{eq} = \varphi ,$$

$$\sum_i (f_i^{eq} - f_i)\mathbf{e}_i = \mathbf{0} \Rightarrow \sum_i f_i^{eq}\mathbf{e}_i = n\mathbf{u} . \tag{10}$$

Following Orlandini et al. [16] and Swift et al. [17] the higher moments of the local equilibrium distribution functions are defined so that we can obtain continuum equations pertinent to a binary fluid mixture. We define

$$\sum_i f_i^{eq} e_{i\alpha} e_{i\beta} = P_{\alpha\beta} + n u_\alpha u_\beta , \tag{11}$$

$$\sum_i g_i^{eq} e_{i\alpha} = \varphi u_\alpha , \tag{12}$$

$$\sum_i g_i^{eq} e_{i\alpha} e_{i\beta} = \Gamma\Delta\mu\delta_{\alpha\beta} + \varphi u_\alpha u_\beta , \tag{13}$$

where Γ is a coefficient related to the mobility of the fluid. We are considering a mixture with the two fluids having the same mechanical properties. The constraint (12) expresses the fact that the two fluids have the same velocity. The local equilibrium distribution functions can be expressed as an expansion in terms of the velocity $\mathbf{u}$ [16,17]:

$$f_0^{eq} = A_0 + C_0 u^2 ,$$

$$f_i^{eq} = A_{\mathrm{I}} + B_{\mathrm{I}} u_\alpha e_{i\alpha} + C_{\mathrm{I}} u^2 + D_{\mathrm{I}} u_\alpha u_\beta e_{i\alpha} e_{i\beta} + G_{\mathrm{I},\alpha\beta} e_{i\alpha} e_{i\beta}, \quad i = 1, 2, 3, 4 \, ,$$

$$f_i^{eq} = A_{\mathrm{II}} + B_{\mathrm{II}} u_\alpha e_{i\alpha} + C_{\mathrm{II}} u^2 + D_{\mathrm{II}} u_\alpha u_\beta e_{i\alpha} e_{i\beta} + G_{\mathrm{II},\alpha\beta} e_{i\alpha} e_{i\beta}, \quad i = 5, 6, 7, 8 \, . \quad (14)$$

Similarly,

$$g_0^{eq} = H_0 + J_0 u^2 \, ,$$

$$g_i^{eq} = H_{\mathrm{I}} + K_{\mathrm{I}} u_\alpha e_{i\alpha} + J_{\mathrm{I}} u^2 + Q_{\mathrm{I}} u_\alpha u_\beta e_{i\alpha} e_{i\beta}, \quad i = 1, 2, 3, 4 \, ,$$

$$g_i^{eq} = H_{\mathrm{II}} + K_{\mathrm{II}} u_\alpha e_{i\alpha} + J_{\mathrm{II}} u^2 + Q_{\mathrm{II}} u_\alpha u_\beta e_{i\alpha} e_{i\beta}, \quad i = 5, 6, 7, 8 \, . \quad (15)$$

Relations (10)–(13) can be used to fix the coefficients of these expansions. The results are reported in the appendix.

2.3. Continuum equations

It has been shown by Orlandini et al. [16] and Swift et al. [17] that the above-described lattice Boltzmann scheme simulates the continuity, the incompressible Navier–Stokes and the convection–diffusion equations. A Chapman–Enskog expansion [17,29] of Eqs. (6) and (7) to $O(\Delta t^2)$ allows to show that

$$v = \frac{(2\tau - 1)}{6}(\Delta t), \quad \Theta = \Delta t \left(\tau_\varphi - \frac{1}{2} \right) . \quad (16)$$

We choose $\tau_\varphi = (1 + 1/\sqrt{3})/2$ in order to minimize the correction terms of order Δt^3. Thus, we are left with two free variables τ and Γ which control the kinematic viscosity v and the macroscopic mobility $\Gamma\Theta$, respectively. All the simulations were run with $\kappa = 1$ (this choice corresponds to an interfacial width of approximately three lattice spacings), $\Gamma\Theta = 0.2$ and units in which $\Delta t = 1$.

3. Shear boundary conditions

The next step in implementing the algorithm is to apply a shear flow on the system. We have modified previous lattice Boltzmann schemes for a single fluid where sliding walls moving in a lattice direction were used to enforce the fluid a given velocity. The flow is assumed to be directed along the *x*-axis (horizontal on the lattice). In this direction, we considered periodic boundary conditions. Then departing distribution functions on outward-pointing links re-enter the lattice via corresponding inward-pointing links on the opposite boundary with no constraint on the macroscopic velocity or density. The walls are on the top and bottom of the lattice. Here one has to face two problems: the correct value of the velocity has to be imposed to the fluid, and the distribution functions pointing outward have to be managed in such a way that mass conservation

for both components and momentum conservation for the bulk are always guaranteed. In the following, we discuss two possible ways for introducing the sliding walls.[1]

3.1. Equilibrium scheme

In the first scheme, we have considered that the boundary walls are placed on the links beyond the upper and the lower sites at a distance equal to half lattice spacing, in the spirit of some works on shear boundary conditions in lattice Boltzmann methods for one fluid [31,32]. We assign to the local equilibrium distributions at the top (t) and the bottom (b) of the lattice the values corresponding to the velocities $w_{x,t} = \gamma(L-1)/2$, $w_{y,t}=0$, $w_{x,b}=-\gamma(L-1)/2$, $w_{y,b}=0$, being $L-1$ the distance between the top and the bottom of the lattice [33]. This method is expected to be accurate for relaxation parameters near unity, since when $\tau = 1$ the collision process (see Eq. (8)) simply replaces the distribution function with the local equilibrium value. For describing the propagation step, let us refer to the upper row and to the f_i's. After a collision, for each site of the upper row, there are three distributions $f_5^c(t)$, $f_2^c(t)$, $f_6^c(t)$ pointing outward the system. The propagation is implemented with the following scheme:

$$f_7(\mathbf{r} + \mathbf{e}_3\Delta t, t + \Delta t) = f_6^c(\mathbf{r}, t),$$

$$f_4(\mathbf{r}, t + \Delta t) = f_2^c(\mathbf{r}, t),$$

$$f_8(\mathbf{r} + \mathbf{e}_1\Delta t, t + \Delta t) = f_5^c(\mathbf{r}, t). \tag{17}$$

This choice can be justified considering reflection of particles against the boundary wall. This allows to guarantee the conservation of mass and momentum, that on each site nine distribution functions are still defined, and that propagation between the adjacent sites on the boundary occurs simultaneously to the propagation on all the inner sites, since $f_5^c(t)$ and $f_6^c(t)$ are propagated over a distance $\sqrt{2}$ in a time step and $f_2^c(t)$ over a distance equal to one. This method, however, as expected and also shown in the following, does not work well for arbitrary values of the relaxation parameters. Therefore, we have developed a second way for introducing the sliding walls.

3.2. Collisional scheme

This second method is an improvement of a scheme proposed by Zou and He [34] for one-fluid systems. In this case, the boundary walls are placed on the upper and lower rows of sites (see, e.g., Refs. [35,36]). We start from the propagation step, as it is realized in the original version by Zou and He [34], and consider again the sites at the top of the lattice. After the propagation, the functions $f_0(t)$, $f_1(t)$, $f_5(t)$, $f_2(t)$, $f_6(t)$

---

[1] A different approach based on Lees–Edwards boundary conditions [30] has been used by Wagner and Yeomans [22]. These boundary conditions, widely used in molecular dynamics, identify the point at (x, y) with the point at $(x + \gamma L\Delta t, y + L)$, where γ is the shear rate. Lattice Boltzmann implementation of Lees–Edwards boundary conditions requires also to change the usual definition of the local equilibrium distribution functions so that we have preferred to use the more straightforward approach with the sliding walls.

and $f_3(t)$ are known on each site of the upper row. One uses Eq. (5) to determine $f_7(t)$, $f_4(t)$, $f_8(t)$ and n. Requiring that the wall velocities $w_{x,t} = \gamma(L-1)/2$, $w_{y,t} = 0$ are imposed to the fluid, we can write

$$f_7(t) + f_4(t) + f_8(t) = n - [f_0(t) + f_1(t) + f_5(t) + f_2(t) + f_6(t) + f_3(t)] \,,$$

$$f_8(t) - f_7(t) = n\gamma \frac{L-1}{2} - [f_1(t) - f_3(t) + f_5(t) - f_6(t)] \,,$$

$$f_7(t) + f_4(t) + f_8(t) = f_5(t) + f_2(t) + f_6(t) \,. \tag{18}$$

Consistency of Eq. (18) gives

$$n = f_0(t) + f_1(t) + f_3(t) + 2[f_2(t) + f_6(t) + f_5(t)] \,. \tag{19}$$

The system of Eq. (18) reduces to two equations with three unknown variables. To close the system of equations the bounce-back rule [31,37] is adopted for the distribution functions normal to the boundary. This means that the value of $f_4(t)$ is fixed assigning to it the known value of its outward-pointing counterpart $f_2(t)$. Then one can solve the system of Eq. (18) finding the solutions

$$f_4(\mathbf{r}, t) = f_2(\mathbf{r}, t) \,,$$

$$f_8(\mathbf{r}, t) = f_6(\mathbf{r}, t) - \frac{1}{2}[f_1(\mathbf{r}, t) - f_3(\mathbf{r}, t)] + \frac{1}{2}n\gamma \frac{L-1}{2} \,,$$

$$f_7(\mathbf{r}, t) = f_5(\mathbf{r}, t) + \frac{1}{2}[f_1(\mathbf{r}, t) - f_3(\mathbf{r}, t)] - \frac{1}{2}n\gamma \frac{L-1}{2} \,. \tag{20}$$

With this choice for the inward-pointing distributions, the desidered momentum at the boundary is achieved. At this point, the collision step is applied to all sites, including the boundary ones. Unfortunately, this scheme does not allow to conserve exactly the total mass due to the fact that the distribution functions $f_5^c(t)$, $f_2^c(t)$ and $f_6^c(t)$ resulting from the collision step are not accounted for any more, and this avoids the exact mass conservation [34].

We have improved the above scheme in order to overcome the mass conservation problem. We consider again the propagation step and the problem of calculating the unknown quantities $f_7(t)$, $f_4(t)$ and $f_8(t)$. After the propagation step on each upper site one has the distribution functions $f_1(t)$, $f_5(t)$, $f_2(t)$, $f_6(t)$ and $f_3(t)$ coming from the nearest sites, $f_0(t - \Delta t)$, which does not propagate, and $f_5(t - \Delta t)$, $f_2(t - \Delta t)$ and $f_6(t - \Delta t)$, all referred to the previous time step, which were lost in the version of Zou and He [34]. Mass will be conserved if the total density n on each site is equal to the quantity $\hat{n}$ given by the sum

$$\hat{n}(t, t - \Delta t) = f_0(t - \Delta t) + f_5(t - \Delta t) + f_2(t - \Delta t) + f_6(t - \Delta t)$$

$$+ f_1(t) + f_5(t) + f_2(t) + f_6(t) + f_3(t) \,. \tag{21}$$

We also require that Eqs. (18) are fulfilled. In order to impose the constraint that on all the boundary sites $n = \hat{n}$, we have to introduce an extra degree of freedom in the
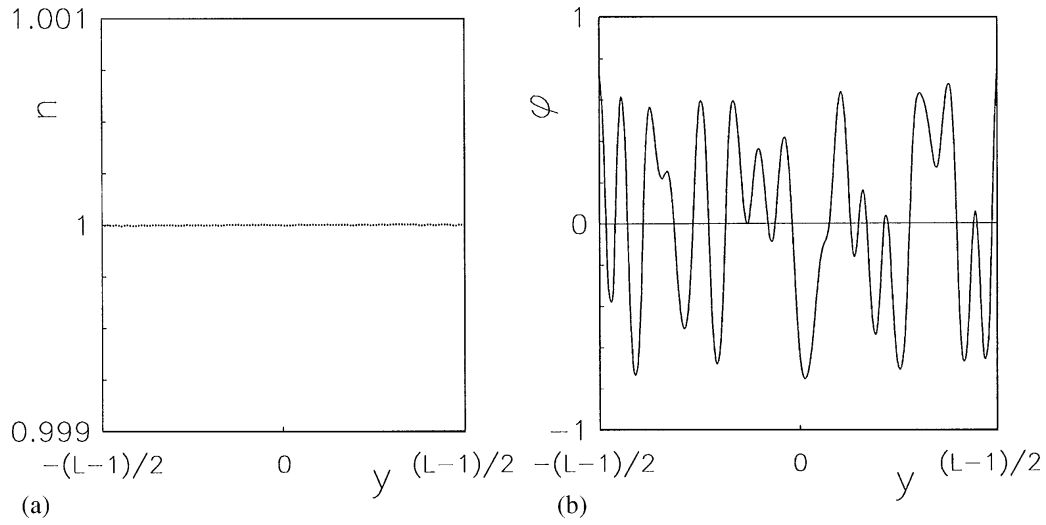
Fig. 2. Plots of the total fluid density n (a) and of the density difference φ (b) along a vertical section at $t = 32$, using the collisional scheme. Simulations were run with $L = 128$, $\gamma = 0.01$ and $\tau = 1$.

system of equations. We have chosen $f_0(t)$ since it does not propagate. The solutions of the system of Eqs. (18), $n = \hat{n}$ and (21) are

$$f_0(\mathbf{r}, t) = \hat{n} - [f_1(\mathbf{r}, t) + f_3(\mathbf{r}, t)] - 2[f_2(\mathbf{r}, t) + f_5(\mathbf{r}, t) + f_6(\mathbf{r}, t)] \qquad (22)$$

and again (20). In this way, it is guaranteed that

$$n(\mathbf{r}, t) = \hat{n}(\mathbf{r}, t, t - \Delta t) \,,$$

$$nu_x(\mathbf{r}, t) = n\gamma \frac{L - 1}{2} \,,$$

$$nu_y(\mathbf{r}, t) = 0 \,. \qquad (23)$$

By this procedure, once the system has been initialized, the application of the propagation and collision steps goes on preserving mass and momentum conservation and implementing the correct velocity values on the boundaries, as it has also been verified numerically.

3.3. Comparison between the two schemes

Here we compare the validity of the two schemes. We have studied how the steady-state velocity profile is reached and we have measured the slip velocity. The shear is applied as usual from the beginning of the phase separation. Preliminarly, we have checked that the boundary conditions do not introduce any artificial discontinuity on the walls. Therefore, we have considered the behaviour of the densities n and φ along vertical sections normal to the flow direction. In Fig. 2(a) and (b), the plots of n and φ, for the middle section of the system, are showed for the collisional scheme. It can be seen that the total density n stays constant and equal to 1 all over the system (its deviations from 1 are less than $1/10^5$) and no boundary effects can be observed. The profile of φ, with the fluctuations corresponding to the presence of
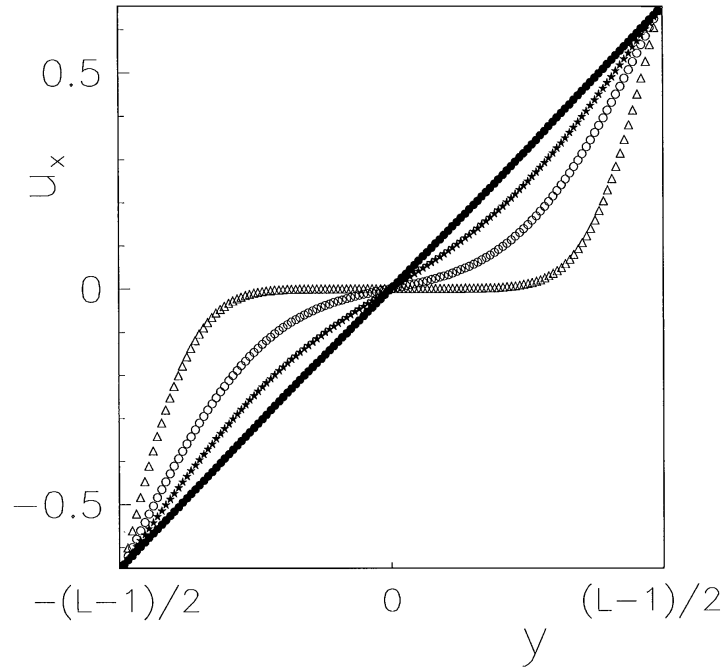
Fig. 3. Plot of the x-component of the fluid velocity as a function of the y-coordinate at consecutive times: ($\triangle$) $t = 2$, ($\bigcirc$) $t = 8$, ($\star$) $t = 16$, ($\bullet$) $t = 32$ for the collisional scheme of shear boundary conditions.

interfaces, does not show anything pathological, as well. Similar results have been obtained with the equilibrium scheme. In Fig. 3, we show at consecutive times the x-component of the fluid velocity along a vertical line in the middle of the system calculated with the collisional scheme. The velocity profiles are independent on the particular vertical section considered. The steady velocity profile is the planar Couette flow [38] with the x-component of the velocity having a linear dependence on the y-coordinate. The evolution of the velocity profile in Fig. 3 is very similar to that observed in simple fluids [39]. The same evolution is obtained with the equilibrium scheme when $\tau = 1$. The situation is different for larger values of τ, when, with the first scheme, the time needed to reach the steady velocity profile is much longer. Actually, it happens that for large enough values of τ the linear profile is not reached before finite-size effects become relevant in the simulations. This can be understood from Eq. (8). Indeed, if $\tau > 1$, $f_i^c(\mathbf{r}, t)$ takes more time to reach the local equilibrium value $f_i^{eq}(\mathbf{r}, t)$ which contains the information about the velocity of walls.

A measure of the time t_r required to reach the steady-state velocity profile can be done in this way. We say that the steady state is reached if

$$\frac{\sum_{\mathbf{r}} |u_x(\mathbf{r}, t + \Delta t) - u_x(\mathbf{r}, t)| + |u_y(\mathbf{r}, t + \Delta t) - u_y(\mathbf{r}, t)|}{\sum_{\mathbf{r}} |u_x(\mathbf{r}, t)| + |u_y(\mathbf{r}, t)|} < T, \tag{24}$$

where T is a tolerance set to 10^{-6}. In Fig. 4, we show the results obtained with the collisional scheme. The time t_r required to reach the steady state decreases at increasing values of τ. The analytic solution of the Navier–Stokes equation for a single fluid subject to a Couette flow suggests a similar behaviour. For a single fluid it can be shown that the non-stationary part of the velocity profile behaves as a series of
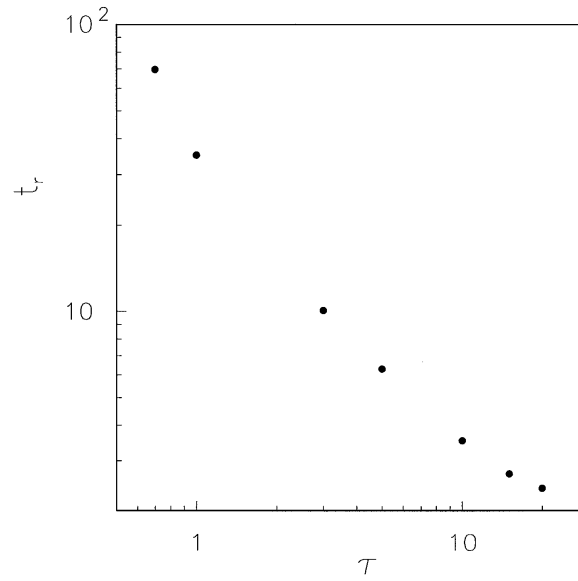
Fig. 4. The time t_r required to reach the steady state is shown as a function of the relaxation parameter τ, using the collisional scheme.
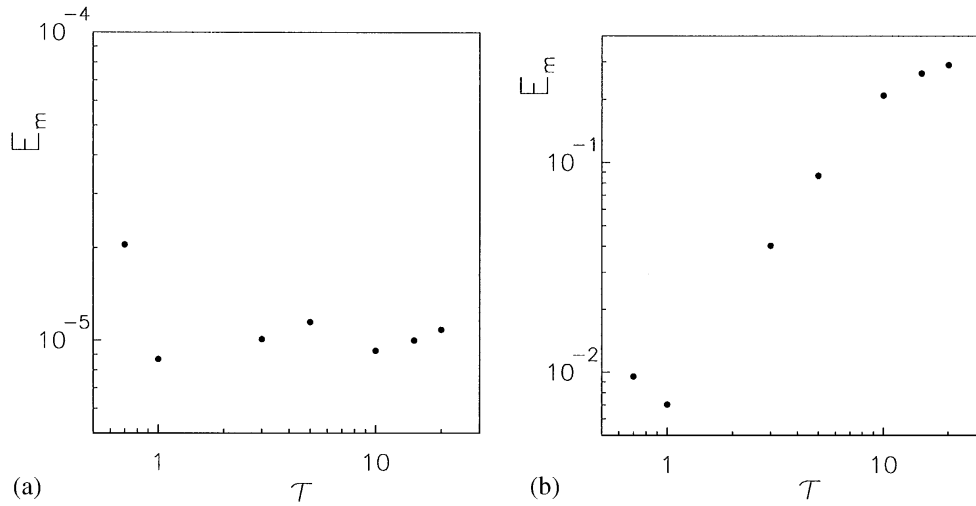

Fig. 5. The maximum relative error E_m in the velocities at the top boundary is reported for the collisional (a) and the equilibrium (b) scheme as a function of τ. Measures were taken at the times shown in Fig. 4.

exponential terms $\exp(-\pi^2 m^2 vt/L^2)$ with m an integer [39]. For this reason we have reported our results in a log–log scale, even if in this plot we do not observe a linear behaviour.

Next, we consider the behaviour of the slip velocity. It is defined as the difference between the wall velocity and the fluid velocity along the wall itself and should be negligible. The slip velocity can be measured by the maximum relative error. At the top boundary it can be calculated as

$$E_m = \max \left| \frac{u_x(i,L) - w_{x,t}}{w_{x,t}} \right|, \quad i = 1, 2, \ldots, L, \tag{25}$$

where again $u_x(i,L)$ is the fluid velocity at the ith site along the x direction at the top boundary and $w_{x,t} = \gamma(L-1)/2$ is the wall velocity. The results of this measure for

different values of τ and for both schemes are presented in Fig. 5. For the collisional scheme $E_m \simeq 10^{-5}$ over the explored range $[0.7, 20]$ of values of τ (Fig. 5(a)). In the equilibrium scheme E_m has a minimum value at $\tau = 1$ and then increases with τ (Fig. 5(b)) arriving to values of order 0.3. The conclusion is that the first scheme gives less convincing results and we have preferred to use the collisional scheme to run our simulations on phase separation.

4. Simulations of phase separation

We have studied the dynamics of phase separation on systems with size $L = 256$, using the values written in Section 2 for the parameters of the model and varying γ in the range $[0.001, 0.01]$ and τ in $[0.7, 5]$.

Here we report the results obtained for $\tau = 0.7$, which corresponds to a viscosity $v = 0.067$, and $\gamma = 0.005$. Similar results have been obtained for other values of parameters. A sequence of configurations at different values of the shear strain γt is shown in the left column of Fig. 6. The first step of the time evolution is the formation of well-defined interfaces. Then, for a while, domains grow isotropically as in the case without shear. At $\gamma t = 0.4$, for example, the effects of the shear can be observed only near the moving walls due to the fact that at this time the linear profile of the velocity is not yet reached and the velocity is greater close to the walls (see Fig. 3). The deformation induced by the flow can be observed everywhere in the system starting from values $\gamma t \simeq 1$. Later on the domains become very stretched and progressively aligned with the flow direction as it can be clearly seen at $\gamma t = 7$ and 11. It is also clear, by looking at these two configurations, that the system shows inhomogeneities and in particular domains with different thicknesses.

A quantitative analysis of the length scales present in the system can be done by considering the behaviour of the structure factor $C(\mathbf{k}, t)$. This quantity is the one of experimental interest being accessible through scattering techniques. It corresponds to the Fourier transform of the two-points correlation function and can be computed numerically as $\langle \varphi(\mathbf{k}, t) \varphi(-\mathbf{k}, t) \rangle$, where $\varphi(\mathbf{k}, t)$ is the Fourier transform of the order parameter $\varphi(\mathbf{r}, t)$ and $\langle \cdots \rangle$ refers to an average over an ensemble of different initial realizations of the system. The wave vector $\mathbf{k}$ in the reciprocal lattice is given by $\mathbf{k} = (2\pi/L)(n_x \mathbf{i} + n_y \mathbf{j})$, where $\mathbf{i}$ and $\mathbf{j}$ are two unit vectors in the k_x and k_y directions, respectively, and n_x and n_y range from $-L/2$ to $L/(2-1)$. It could be useful to remind the behaviour of $C(\mathbf{k}, t)$ in the case without shear. Its shape is that of a volcano with a contour plot similar to that shown in Fig. 6 at $\gamma t = 0.4$. The radius of the volcano defines the inverse of a characteristic length representing the average size of domains at a given time. As time goes by, the height of this volcano increases while its support shrinks towards the origin. This means that the characteristic length scale associated with the size of domains increases and the system is more and more ordered on that scale. The fact that the structure factor is circular reflects the isotropy of the system.

The shear affects in a significant way the evolution of the structure factor. At $\gamma t = 1$ the shape of the volcano is deformed into an elliptical structure as it can be seen in
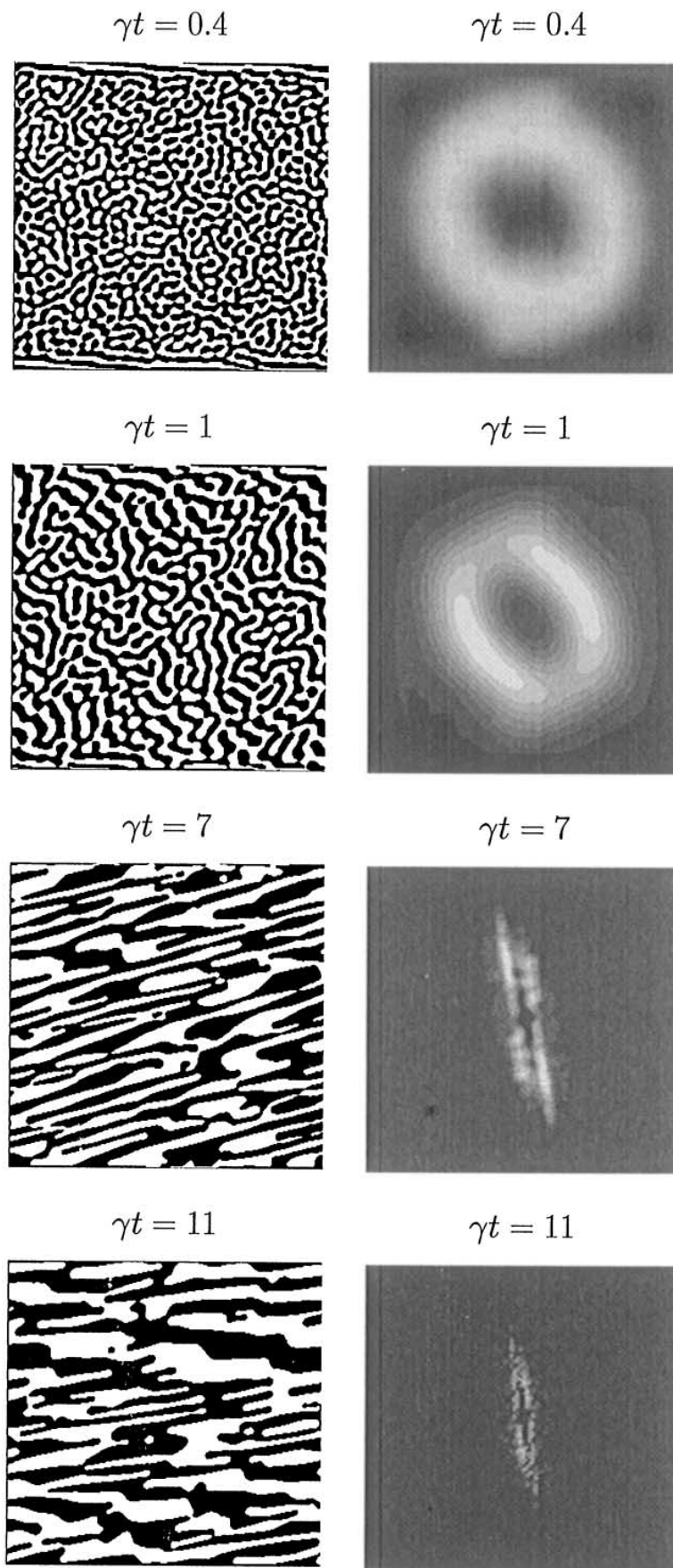
$\gamma t = 0.4$ $\gamma t = 0.4$

$\gamma t = 1$ $\gamma t = 1$

$\gamma t = 7$ $\gamma t = 7$

$\gamma t = 11$ $\gamma t = 11$

Fig. 6. Configurations of the system are shown in the left column at different values of the shear strain γt. In the right column the structure factor is contour-plotted at the same values of γt.

the contour plot of Fig. 6. Moreover, also the profile of the edge of the volcano is deformed and two maxima can be observed distributed around the main diagonal of the k_x–k_y plane. In the further evolution, the two broad maxima at $\gamma t = 1$ become divided into two separate foils and on each foil two different peaks can be observed. This can be clearly seen at $\gamma t = 7$. These two foils becomes closer and closer to the axis $k_x = 0$ and increasingly more aligned along the k_y-axis. This pattern corresponds to interfaces very elongated in the direction of the flow as it appears in the corresponding pictures of configurations.

The presence of two peaks on each foil implies the existence of different length scales in the systems. Due to the symmetry $C(\mathbf{k}, t) = C(-\mathbf{k}, t)$ the two foils are perfectly symmetric and it is sufficient to consider only the two peaks of one foil. Therefore, for each direction there are two relevant length scales. Focussing on what happens in the direction normal to the flow we arrive to the conclusion that there are domains with two characteristic thicknesses in the system. This better explains the inhomogeneities observed in the configurations at $\gamma t = 7$ and 11.

Also, the dynamical evolution of the four-peaked structure factor is very peculiar. At $\gamma t = 7$, the peaks which prevail are the ones with a larger value of k_y. This corresponds to a prevalence of thin domains in the system, as it can perhaps be observed by directly looking at the corresponding configuration. Later on the more isotropic peak with the smaller value of k_y, which has grown faster than the other, becomes higher. This can be observed in Fig. 6 at $\gamma t = 11$ in correspondence of a larger abundance of thicker domains.

The physical picture of what happens in the system is the following. By stretching the interfaces the shear induces a stress in the system. This stress increases more and more producing a prevalence of thin domains. At a certain point the domains are broken by the flow in points where the stress is larger. This occurs in a cooperative way with a sequence of ruptures producing domains which are less stretched. Then the thicker domains, not yet broken by the flow, become more numerous and the more isotropic peak of $C(\mathbf{k}, t)$ dominates as at $\gamma t = 11$. It was not possible to follow longer in our simulations the alternate predominance of the two peaks due to inevitable appearance of finite-size effects. Previous analytical results of Corberi et al. [11] show that in the diffusive regime the alternate prevalence of the two peaks continues periodically on a logarithmic time scale. We cannot give results on this. Here we mention that in experiments with polymer solutions by Migler et al. [40], after a shallow quench under the critical temperature, segregation is observed with four-peaked structure factors similar to those of Fig. 6. Moreover, in previous experimental papers [41–43] always on polymer solutions, the description of the dynamics of the network of domains is similar to that given above. We believe that our simulations, where for the first time the presence of two length scales is considered, help to understand these experimental facts.

We conclude this section giving the results of an explicit evaluation of the size of the domains. This measure is usually obtained from the momenta of the structure factor. Since our system is anisotropic, we define the average size of domains in the
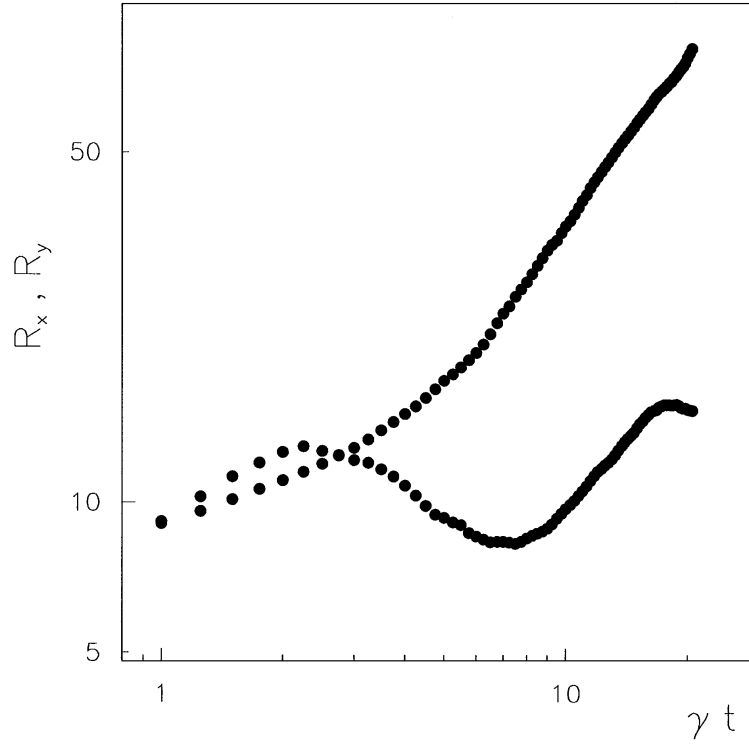
Fig. 7. Evolution of the average domain size in the shear (lower curve) and flow (upper curve) directions. The slope of R_x is 1.1.

flow direction as

$$R_x(t) = \pi \frac{\int d\mathbf{k} C(\mathbf{k}, t)}{\int d\mathbf{k} |k_x| C(\mathbf{k}, t)} \qquad (26)$$

and analogously for $R_y(t)$, in the shear direction normal to the flow. They are one half of the wavelength corresponding to the characteristic wave vector. In the case without shear lattice Boltzmann simulations with our parameters give $R_x = R_y \sim t^{2/3}$ [19]. $\alpha = \frac{2}{3}$ is the value of the growth exponent typical of the inertial regime which occurs at very low viscosity [44]. From our simulations, we extract the behaviour shown in Fig. 7. As in all the other simulations with a shear flow [14,15], it has not been possible to extract the value of the exponent α due to the relevance of finite-size effects.[2] Using an argument proposed by Corberi et al. [12], based on a renormalization group approach [46], one should expect in the present case, if dynamical scaling for the structure factor holds, that the growth in the shear direction obeys the same power law as in the case without shear, $R_y(t) \sim t^{2/3}$, while in the x-direction $R_x(t) \sim \gamma t R_y(t) \sim \gamma t^{5/3}$. This means that the growth exponent α_x in the flow direction is related to α_y, the growth exponent in the shear direction, by the relation $\alpha_x = \alpha_y + 1$, where the extra contribution 1 with respect to the unsheared case comes from the convective term in the convection–diffusion equation. Our runs, performed on an Alpha Workstation XP1000 with 1 GB of RAM, do not allow to check these predictions. The results of Fig. 7 can be more

---

[2] An analytical determination of the exponent α is only available for the diffusive regime [11,45]. It is found that $\alpha = \frac{4}{3}$ in the flow direction, and $\alpha = \frac{1}{3}$ in the other directions as in the case without shear.

easily related to the above-discussed dynamical behaviour of the structure factor with the alternate dominance of the two peaks which corresponds to the oscillatory pattern of R_x and R_y. We also observe that these oscillations make more difficult a possible evaluation of the growth exponents.

5. Conclusions

We studied phase separation in sheared binary fluid mixtures at low viscosity. We introduced proper boundary conditions to impose the shear flow on the system. These boundary conditions strictly conserve mass and momentum and do not introduce any appreciable slip velocity. Our main results show that the network of domains is characterized by the existence of two typical length scales for each direction. Indeed, domains with different thickness are clearly visible in the simulations. Structure factors with four peaks confirm these observations. During the time evolution there is an alternate dominance of two of these peaks over the other couple. This corresponds to a larger abundance first of thin and later of thicker domains. Simulations on much larger scales are needed to establish if the oscillations of the peaks only characterize an initial transient or if they continue indefinitely, as it is suggested by the results of Corberi et al. [11] valid for the diffusive regime at infinite viscosity.

Acknowledgements

Appendix

A suitable choice of the coefficients in expansions (14), (15) consistent with conditions (10)–(13) is

$$A_0 = n - 20A_{\mathrm{II}}, \quad A_{\mathrm{I}} = 4A_{\mathrm{II}}, \quad A_{\mathrm{II}} = \frac{P_{xx} + P_{yy}}{24} \,, \tag{A.1}$$

$$B_{\mathrm{I}} = 4B_{\mathrm{II}}, \quad B_{\mathrm{II}} = \frac{n}{12} \,, \tag{A.2}$$

$$C_0 = -\frac{2n}{3}, \quad C_{\mathrm{I}} = 4C_{\mathrm{II}}, \quad C_{\mathrm{II}} = -\frac{n}{24} \,, \tag{A.3}$$

$$D_{\mathrm{I}} = 4D_{\mathrm{II}}, \quad D_{\mathrm{II}} = \frac{n}{8} \,, \tag{A.4}$$

$$G_{\mathrm{I},\alpha\beta} = 4G_{\mathrm{II},\alpha\beta}, \quad G_{\mathrm{II},xx} = -G_{\mathrm{II},yy} = \frac{P_{xx} - P_{yy}}{16}, \quad G_{\mathrm{II},xy} = -G_{\mathrm{II},yx} = \frac{P_{xy}}{8} \,, \tag{A.5}$$

$$H_0 = \varphi - 20H_{\mathrm{II}}, \quad H_{\mathrm{I}} = 4H_{\mathrm{II}}, \quad H_{\mathrm{II}} = \frac{\Gamma \Delta \mu}{12}, \tag{A.6}$$

$$K_{\mathrm{I}} = 4K_{\mathrm{II}}, \quad K_{\mathrm{II}} = \frac{\varphi}{12}, \tag{A.7}$$

$$J_0 = -\frac{2\varphi}{3}, \quad J_{\mathrm{I}} = 4J_{\mathrm{II}}, \quad J_{\mathrm{II}} = -\frac{\varphi}{24}, \tag{A.8}$$

$$Q_{\mathrm{I}} = 4Q_{\mathrm{II}}, \quad Q_{\mathrm{II}} = \frac{\varphi}{8}. \tag{A.9}$$

References

[1] J.D. Gunton, M. San Miguel, P.S. Sahni, in: C. Domb, J.L. Lebowitz (Eds.), Phase Transitions and Critical Phenomena, Academic, New York, 1983.
[2] A. Onuki, J. Phys.: Condens. Matter 9 (1997) 6119.
[3] T. Hashimoto, K. Matsuzaka, E. Moses, A. Onuki, Phys. Rev. Lett. 74 (1995) 126.
[4] T. Ohta, H. Nozaki, M. Doi, Phys. Lett. A 145 (1990) 304.
[5] T. Ohta, H. Nozaki, M. Doi, J. Chem. Phys. 93 (1990) 2664.
[6] D.H. Rothman, Europhys. Lett. 14 (1991) 337.
[7] J.F. Olson, D.H. Rothman, J. Stat. Phys. 81 (1995) 199.
[8] Y.N. Wu, H. Skrdla, T. Lookman, S.Y. Chen, Physica A 239 (1997) 428.
[9] P. Padilla, S. Toxvaerd, J. Chem. Phys. 106 (1997) 2342.
[10] Z. Shou, A. Chakrabarti, Phys. Rev. E 61 (2000) R2200.
[11] F. Corberi, G. Gonnella, A. Lamura, Phys. Rev. Lett. 81 (1998) 3852.
[12] F. Corberi, G. Gonnella, A. Lamura, Phys. Rev. Lett. 83 (1999) 4057.
[13] A.J. Bray, Adv. Phys. 43 (1994) 357.
[14] J.M. Yeomans, Annu. Rev. Comput. Phys. VII (2000).
[15] J.M. Yeomans, in: D. Stauffer (Ed.), Annual Review of Computational Physics, in press.
[16] E. Orlandini, M.R. Swift, J.M. Yeomans, Europhys. Lett. 32 (1995) 463.
[17] M.R. Swift, E. Orlandini, W.R. Osborn, J.M. Yeomans, Phys. Rev. E 54 (1996) 5041.
[18] S. Chen, G.D. Doolen, Annu. Rev. Fluid Mech. 30 (1998) 329.
[19] W.R. Osborn, E. Orlandini, M.R. Swift, J.M. Yeomans, J.R. Banavar, Phys. Rev. Lett. 75 (1995) 4031.
[20] V.M. Kendon, J.C. Desplat, P. Bladon, M.E. Cates, Phys. Rev. Lett. 83 (1999) 576.
[21] G. Gonnella, E. Orlandini, J.M. Yeomans, Phys. Rev. Lett. 78 (1997) 1695.
[22] A.J. Wagner, J.M. Yeomans, Phys. Rev. E 59 (1999) 4366.
[23] M.E. Cates, V.M. Kendon, P. Bladon, J.C. Desplat, Faraday Discuss. 112 (1999) 1.
[24] J.S. Rowlinson, B. Widom, Molecular Theory of Capillarity, Clarendon Press, Oxford, 1982.
[25] A.J.M. Yang, P.D. Fleming, J.H. Gibbs, J. Chem. Phys. 64 (1976) 3732.
[26] R. Evans, Adv. Phys. 28 (1979) 143.
[27] P. Bhatnagar, E.P. Gross, M.K. Krook, Phys. Rev. 94 (1954) 511.
[28] H. Chen, S. Chen, W. Matthaeus, Phys. Rev. A 45 (1992) R5339.
[29] S. Chapman, T. Cowling, The Mathematical Theory of Non-uniform Gases, Cambridge University Press, Cambridge, 1970.
[30] A.W. Lees, S.F. Edwards, J. Phys. C 5 (1972) 1921.
[31] R. Cornubert, D. d'Humieres, D. Levermore, Physica D 47 (1991) 241.
[32] A.J. Ladd, J. Fluid Mech. 271 (1994) 285.
[33] X. He, Q. Zou, L.S. Luo, M. Dembo, J. Stat. Phys. 87 (1997) 115.
[34] Q. Zou, X. He, Phys. Fluids 9 (1997) 1591.
[35] D.R. Noble, S. Chen, J.G. Georgiadis, R.O. Buckius, Phys. Fluids 7 (1995) 203.
[36] T. Inamuro, M. Yoshino, F. Ogino, Phys. Fluids 7 (1995) 2928.
[37] P. Lavallée, J. Boon, A. Noullez, Physica D 47 (1991) 233.
[38] L.D. Landau, E.M. Lifshitz, Fluid Mechanics, Pergamon Press, Oxford, 1959.

[39] H. Schlichting, Boundary Layer Theory, McGraw-Hill series in Mechanical Engineering, 1979.

[40] K. Migler, C. Liu, D.J. Pine, Macromolecules 29 (1996) 1422.

[41] Z. Laufer, H.L. Jalink, A.J. Staverman, J. Polym. Sci. 11 (1973) 3005.

[42] S. Mani, M.F. Malone, H.H. Winter, J.L. Halary, L. Monnerie, Macromolecules 24 (1991) 5451.

[43] S. Mani, M.F. Malone, H.H. Winter, Macromolecules 25 (1992) 5671.

[44] H. Furukawa, Adv. Phys. 34 (1985) 703.

[45] N.P. Rapapa, A.J. Bray, Phys. Rev. Lett. 83 (1999) 3856.

[46] A.J. Bray, Phys. Rev. B 41 (1990) 6724.